





















Analysing the Onset of Cometary Activity by the Jupiter-Family Comet 2023 RN₃

MATTHEW M. DOBSON ¹, MEGAN E. SCHWAMB ¹, ALAN FITZSIMMONS ¹, MICHAEL S. P. KELLEY ²,
CARRIE E. HOLT ³, JOSEPH MURTAGH ¹, HENRY H. HSIEH ^{4,5}, LARRY DENNEAU ⁶, NICOLAS ERASMUS ⁷,
A. N. HEINZE ⁸, LUKE J. SHINGLES ^{9,1}, ROBERT J. SIVERD ⁶, KEN W. SMITH ¹, JOHN L. TONRY ⁶,
HENRY WEILAND ⁶, DAVID. R. YOUNG ¹, TIM LISTER ³, EDWARD GOMEZ ¹⁰, JOEY CHATELAIN ³ AND
SARAH GREENSTREET ^{11,8}

¹*Astrophysics Research Centre, School of Mathematics and Physics, Queen's University Belfast, Belfast BT7 1NN, UK*

²*Department of Astronomy, University of Maryland, College Park, MD 20742-0001, USA*

³*Las Cumbres Observatory, 6740 Cortona Drive Suite 102, Goleta, CA 93117, USA*

⁴*Planetary Science Institute, 1700 East Fort Lowell Rd., Suite 106, Tucson, AZ 85719, USA*

⁵*Institute of Astronomy and Astrophysics, Academia Sinica, P.O. Box 23-141, Taipei 10617, Taiwan*

⁶*Institute for Astronomy, University of Hawaii at Manoa, Honolulu, HI 96822, USA*

⁷*South African Astronomical Observatory, Cape Town 7925, South Africa*

⁸*Department of Astronomy and the DIRAC Institute, University of Washington, 3910 15th Ave NE, Seattle, WA 98195, USA*

⁹*GSI Helmholtzzentrum für Schwerionenforschung, Planckstraße 1, 64291 Darmstadt, Germany*

¹⁰*Las Cumbres Observatory, School of Physics and Astronomy, Cardiff University, Queens Buildings, The Parade, Cardiff CF24 3AA, UK*

¹¹*Rubin Observatory/NSF NOIRLab, 950 N. Cherry Ave, Tucson, AZ 85719, USA*

ABSTRACT

We utilize serendipitous observations from the Asteroid Terrestrial-impact Last Alert System (ATLAS) and the Zwicky Transient Facility (ZTF) in addition to targeted follow-up observations from the Las Cumbres Observatory (LCO) and Liverpool Telescope to analyze the first observed instance of cometary activity by the newly-discovered Jupiter-family comet C/2023 RN₃ (ATLAS), whose orbital dynamics place it close to residing on a Centaur-like orbit. Across our 7-month baseline, we observe an epoch of cometary activity commencing in August 2023 with an increase in brightness of >5.4 mag. The lightcurve of 2023 RN₃ indicates the presence of continuous cometary activity across our observations, suggesting the onset of a new period of sustained activity. We find no evidence of any outbursts on top of the observed brightening, nor do we find any significant color evolution across our observations. 2023 RN₃ is visibly extended in LCO and Liverpool Telescope observations, indicating the presence of a spatially-extended coma. Numerical integration of 2023 RN₃'s orbit reveals the comet to have recently undergone a slight increase in semimajor axis due to a planetary encounter with Jupiter, however whether this orbital change could trigger 2023 RN₃'s cometary activity is unclear. Our estimate for the maximum dust production metric of $Afp \sim 400$ cm is consistent with previous measurements for the Jupiter-family comet and Centaur populations.

1. INTRODUCTION

C/2023 RN₃ (ATLAS) (hereafter referred to as “2023 RN₃”) is a Jupiter-family comet (JFC) recently discovered by the Asteroid Terrestrial-impact Last Alert System (ATLAS; Tonry et al. 2018a,b) wide-field sky survey on 2023 September 4 (Green 2023) during an epoch of cometary activity which caused it to brighten by more than 4 magnitudes (Hsieh et al. 2023). Early analysis of 2023 RN₃'s cometary activity by Hsieh et al. (2023) revealed the presence of a visible coma. With a semimajor axis $a = 10.147$ au, perihelion $q = 5.172$ au (last passed on 2023 January 16), eccentricity $e = 0.490$, and inclination $i = 10.358$ deg, 2023 RN₃'s orbit is that of a JFC, with a Tisserand parameter

$T_J = 2.907$. However, its perihelion and Tisserand parameter values lie close to the threshold values ($q = 5.2$ au (Jewitt 2009; Gladman et al. 2008) and $T_J = 3.05$ (Gladman et al. 2008), respectively) that separate the JFC population from the Centaurs, small icy objects on chaotic orbits in the giant planet region of the solar system that are thought to replenish the JFC population, making the study of 2023 RN₃ relevant to studies of both JFCs and Centaurs.

Both Centaurs and JFCs are known to exhibit cometary activity (Jewitt 2009; Kelley & Wooden 2009; Bauer et al. 2013; Peixinho et al. 2020; Jewitt & Hsieh 2022), manifesting as dust comae and tails. This activity can take the form of ‘outbursts’, sudden and brief increases in the mass-loss and corresponding brightness of the object (Hughes 1990). However, while the activity of Jupiter-family comets is closely coupled with their proximity to perihelion, the activity exhibited by Centaurs can occur throughout their orbits (Peixinho et al. 2020). This points to different mechanisms responsible for activity exhibited by both populations. The activity of Jupiter-family comets is generally due to the sublimation of water ice for those with perihelia interior to ~ 3 au (Meech & Svoren 2004; Womack et al. 2017), with sublimation of CO and CO₂ thought to be the dominant driver of JFC activity exterior to this distance (Ootsubo et al. 2012; Cochran et al. 2015). By comparison, the mechanism responsible for Centaur activity is not as well understood. Proposed causes of Centaur activity include newly-exposed pockets of volatile surface ices (Prialnik 1992) or volatiles released by the amorphous-to-crystalline transition of sub-surface water ice (Jewitt 2009). Furthermore, analysis of Centaur orbital dynamics points to correlations between the activity exhibited by a Centaur and its perihelion (Jewitt 2009; Lilly et al. 2021), its lifetime in the giant planet region (Fernández et al. 2018), and its evolutionary history, with active Centaurs tending to have encountered a giant planet in the last $\sim 10^3$ years of its history, causing an abrupt decrease in its semimajor axis (Fernández et al. 2018; Lilly et al. 2021, 2024). Understanding the mechanism behind Centaur activity, and how this activity transitions to that exhibited by Jupiter-family comets, is thus an important step in understanding cometary evolution in the solar system.

In this paper, we analyze the 2023 cometary activity of 2023 RN₃, combining follow-up observations from Las Cumbres Observatory (LCO, Brown et al. 2013) as part of the Las Cumbres Observatory Outbursting Objects Key (LOOK; Lister et al. 2022) project and the Liverpool Telescope (Steele et al. 2004) along with serendipitous observations from ATLAS and the Zwicky Transient Facility (ZTF; Bellm et al. 2019; Graham et al. 2019). This paper is structured as follows: in Section 2, we briefly describe the observations used in our analysis and photometry. In Section 3 we present our analysis and findings studying the evolution in the brightness, color, radial profile, and dust production of 2023 RN₃. We present our summary and conclusions in Section 4.

2. OBSERVATIONS AND DATA REDUCTION

Our dataset consists of both targeted follow-up observations of 2023 RN₃ (LOOK and Liverpool Telescope) and serendipitous observations of the object from automated surveys (ATLAS and ZTF). Our observations, summarised in Table 1, extend in time from 2023 June 6 to 2024 February 2. The serendipitous observations from ATLAS and ZTF make up the majority of our dataset, and cover the onset of 2023 RN₃’s cometary activity first observed on 2023 August 26 (see Section 3.1). Our observations from LOOK and Liverpool telescope sample 2023 RN₃ after its activity commenced.

2.1. ATLAS

ATLAS regularly observes the entire night sky to a limiting magnitude of 19.5 mag using 30-second exposures in two non-standard filters, cyan (*c*, 420-650 nm) and orange (*o*, 560-820 nm) (Tonry et al. 2018a). ATLAS consists of four telescope units, two of which are located in Hawai’i (Mauna Loa and Haleakala), one in Chile (El Sauce) and one in South Africa (Sutherland). Each of the four ATLAS units consists of a 0.5-m Schmidt telescope with a field of view (FOV) of 28.9 square degrees with a pixel scale of 1.86 arcsec/pixel (Tonry et al. 2018a,b). Further details of ATLAS and its data reduction pipeline can be found in Tonry et al. (2018a,b), and Smith et al. (2020). We use both *c* and *o* filter observations of 2023 RN₃ from all four ATLAS telescopes between 2023 June 6 and 2024 February 2. We utilize the difference images automatically generated by the ATLAS reduction pipeline for each observation, to reduce the effect of contamination from background flux sources (e.g. stars, galaxies) on our photometry of 2023 RN₃.

2.2. ZTF

Using the 48-inch (1.2-m) Samuel Oshin telescope, the Zwicky Transient Facility (ZTF) is a wide-field time domain survey which has been observing the visible sky since 2017 October with a cadence of approximately three days. Each

Table 1. Number and Time Ranges of Observations of 2023 RN₃ for Each Filter Used in our Analysis

Telescope/Survey	Filter	Start Date (YYYY-MM-DD)	End Date (YYYY-MM-DD)	Number of Observations
ATLAS	<i>c</i>	2023-07-18	2023-12-10	36
ATLAS	<i>o</i>	2023-06-06	2023-12-16	106
ZTF	ZTF- <i>g</i>	2023-08-03	2023-11-13	26
ZTF	ZTF- <i>r</i>	2023-08-03	2024-01-05	28
Liverpool Telescope	SDSS- <i>g'</i>	2023-12-08	2023-12-14	6
Liverpool Telescope	SDSS- <i>r'</i>	2023-11-26	2023-12-14	11
Liverpool Telescope	SDSS- <i>i'</i>	2023-11-26	2023-12-14	12
LOOK	PS1 <i>w</i>	2023-11-17	2023-11-17	4
LOOK	SDSS- <i>g'</i>	2023-11-16	2024-01-10	26
LOOK	SDSS- <i>r'</i>	2023-11-16	2024-01-10	24
LOOK	SDSS- <i>i'</i>	2023-11-26	2024-01-10	19
Total		2023-06-06	2024-01-10	298

observation has an exposure time of 30-seconds, with a FOV of 43 square degrees and a pixel scale of 1.01 arcsec/pixel, and are obtained using three broadband filters ZTF-*g*, ZTF-*r*, and ZTF-*i*. Further details of ZTF, its system overview, survey strategy, data processing pipeline, and science objectives can be found in [Bellm et al. \(2019\)](#), [Graham et al. \(2019\)](#), and [Masci et al. \(2019\)](#). We query the ZTF observations of 2023 RN₃ via the Infrared Science Archive (IRSA) of the National Aeronautics and Space Administration (NASA) Infrared Processing and Analysis Center (IPAC), which utilizes the Jet Propulsion Laboratory (JPL) Horizons¹ ephemeris of a queried object to obtain all ZTF observations which coincide with the position of that object. These observations range in time from 2023 August 3 to 2024 January 7 in the broadband filters ZTF-*g* and ZTF-*r*.

2.3. LOOK

The Las Cumbres Observatory (LCO) 1.0-m telescopes ([Brown et al. 2013](#)) observed 2023 RN₃ from 2023 November 26 to 2024 January 10 (including the observations reported in [Hsieh et al. 2023](#)) as part of the LCO Outbursting Objects Key Project (LOOK; [Lister et al. 2022](#)). Observations were taken in SDSS *g*, *r*, and *i* filters ([Chambers et al. 2016](#)) with the original [Hsieh et al. \(2023\)](#) observations in the *w*-filter included in our analysis. Observations were scheduled with the NEOExchange web portal ([Lister et al. 2021](#)). Each 1-m telescope utilizes an identical Sinistro imager comprising a Fairchild 4096 × 4096 pixel charge-coupled device CCD with a field of view of 26.6' × 26.6', resulting in a pixel scale of 0.387 arcsec/pixel ([Brown et al. 2013](#)). To ensure negligible on-sky motion of 2023 RN₃ within this pixel scale, all observations were obtained with the telescope in half-rate tracking mode, with exposure times of 245 seconds. These observations are automatically processed using the LCO image processing pipeline “Beautiful Algorithm to Normalize Zillions of Astronomical Images” (BANZAI; [McCully et al. 2018](#)). The LOOK photometry pipeline includes automatic calibration of observations to the Pan-STARRS1 photometric system ([Tonry et al. 2012](#)) using the ATLAS-RefCat2 all-sky photometric catalog ([Tonry et al. 2018b](#)), the CALVIACAT software ([Kelley & Lister 2021](#)), and background field stars measured with BANZAI ([Lister et al. 2022](#)). Due to the difference between the Pan-STARRS1 filter system of ATLAS-RefCat2 and the SDSS filter system of LCO, the LOOK photometry pipeline performs a color correction to transform the instrumental magnitudes to their corresponding Pan-STARRS1 filters *g'*, *r'*, and *i'* ([Lister et al. 2022](#)). Of these observations, we utilize for our analysis only those which were obtained with seeing ≤ 4 arcsec.

2.4. Liverpool Telescope

¹ <https://ssd.jpl.nasa.gov>

The Liverpool Telescope is a 2-m robotic telescope located at the Observatorio del Roque de los Muchachos, La Palma, Canary Islands (Steele et al. 2004). We obtained observations of 2023 RN₃ between 2023 November 26 and 2023 December 14 using the IO:O wide-field camera (Barnsley et al. 2016) whose 4096×4112 pixel CCD results in a field of view $10' \times 10'$. Observations were obtained in SDSS r and i filters for conditions of airmass < 2.0 and seeing < 2.0 arcsec. We utilize sidereal tracking of 2023 RN₃, with exposure times of 82 seconds for g filter observations and 70 seconds in r and i filters to ensure negligible on-sky motion of the object within the 0.3 arcsec/pixel resolution afforded by 2x2 pixel binning. Observations were automatically reduced via the IO:O reduction pipeline. We analyze 2023 RN₃ in the 29 observations where it was detected above 3σ .

3. ANALYSIS AND RESULTS

Our multi-wavelength observations from ATLAS, ZTF, LOOK, and Liverpool Telescope allow us to analyze 2023 RN₃'s 2023 cometary activity. We use the multi-month, multi-wavelength baseline observations from ATLAS, ZTF, and LOOK to explore the evolution of 2023 RN₃'s measured brightness and determine any evolution of its observed color. We use the high-resolution LOOK and Liverpool Telescope observations to analyze 2023 RN₃'s surface brightness distribution across time. Finally, we utilize our ATLAS, ZTF, and LOOK observations to estimate 2023 RN₃'s activity level across our observational baseline.

3.1. Brightness Evolution

Using our largest datasets, ATLAS, ZTF, and LOOK, we examine the brightness evolution of 2023 RN₃. To account for the visible extension exhibited by 2023 RN₃ as reported by Hsieh et al. (2023), we perform aperture photometry on all our observations with a sufficiently large aperture, applying an effective radius of 20,000 km, corresponding to an angular size of $4.83''$ to $6.36''$ across our observations. We use the aperture photometry automatically calculated by the LOOK photometry pipeline (Lister et al. 2022). For our ATLAS and ZTF observations, we use Source Extractor Python (Bertin & Arnouts 1996; Barbary 2016) to identify sources. We identify the closest source as 2023 RN₃ within a threshold distance (3 arcsec for ATLAS observations, 1.5 arcsec for ZTF, due to the differing pixel scales of both surveys) from 2023 RN₃'s predicted position by JPL Horizons. We use the *photutils* Python library (Bradley 2023) to perform aperture photometry on 2023 RN₃, applying a circular aperture. The background annulus apertures had inner and outer radii of 4 and 5 times the circular aperture radius, 20,000 km, respectively. We apply per observation the zeropoints reported from the ATLAS (Tonry et al. 2018b) and ZTF (Masci et al. 2019) photometry pipelines. If the flux measured for 2023 RN₃ has a signal-to-noise ratio (SNR) of < 3 , or if no source is found by Source Extractor Python, we calculate a 3σ upper limit $m_{3\sigma}$ from forced photometry at the predicted coordinates of 2023 RN₃ according to the equation:

$$M_{3\sigma} = -2.5 \log_{10}(3 * dF) + ZP \quad (1)$$

where dF is the uncertainty in the measured flux and ZP is the observation zeropoint magnitude. Table 2 lists the magnitude measurements (or 3σ upper limits) of 2023 RN₃ for each observation on which we performed photometry.

To transform our magnitude measurements to the same wavelength, we select the ATLAS o filter dataset as our standard filter on account of it having the largest number of observations and the longest time baseline, calculating and applying a color offset to the other datasets (listed in Table 3). Magnitude offsets were calculated from the difference in median apparent magnitude between a given filter and the ATLAS o filter across their overlapping timespan. For each color-corrected magnitude value, we query JPL Horizons for the corresponding geocentric and heliocentric distances of 2023 RN₃ at the time of observation and transform the apparent magnitudes of 2023 RN₃ into reduced magnitudes (the apparent magnitude scaled to geocentric and heliocentric distances of 1 au). Figure 1 shows the apparent magnitude lightcurves of 2023 RN₃ in each filter, with the magnitudes standardized for the o -filter shown in Figure 2. The serendipitous datasets from ATLAS and ZTF allowed them to sample the rise of 2023 RN₃'s brightness, with ZTF making the first detection on 2023 August 26 and ATLAS making the last non-detection on 2023 August 21; targeted follow-up observations from LOOK were scheduled after the object was detected. Figures 1 and 2 show that over the course of 137 days, 2023 RN₃ suddenly increased in brightness at an initial rate of approximately 0.36 mag/day, reaching a peak apparent brightness of ~ 17.5 mag, and has since levelled off to a constant magnitude after a slight decrease in brightness. This indicates that cometary activity may be continuing across this period and that 2023 RN₃'s increase in brightness is the onset of an epoch of continuous cometary activity. Extrapolating 2023 RN₃'s

Table 2. Apparent Magnitudes of 2023 RN₃ in Each Observation from ATLAS, ZTF, and LOOK.

MJD	Magnitude	Magnitude	Photometry	Filter	Heliocentric	Geocentric	Phase Angle	Survey
		Uncertainty	Flag		Distance	(au)	Distance	
	(mag)	(mag)			(au)	(au)	(deg)	
60191.567824	17.683	0.084	1	o	5.312	4.377	4.5017	ATLAS
60191.571448	17.875	0.100	1	o	5.312	4.377	4.5011	ATLAS
60191.604028	17.783	0.099	1	o	5.312	4.377	4.4952	ATLAS
60204.173872	17.677	0.065	1	o	5.327	4.339	2.1776	ATLAS
60204.177039	17.635	0.062	1	o	5.327	4.339	2.1770	ATLAS
60204.179792	17.821	0.087	1	o	5.327	4.339	2.1765	ATLAS
60204.210026	17.660	0.071	1	o	5.327	4.339	2.1711	ATLAS
60213.104433	17.628	0.108	1	o	5.339	4.339	0.9948	ATLAS
60213.127136	17.588	0.101	1	o	5.339	4.339	0.9942	ATLAS
60213.140634	17.678	0.108	1	o	5.339	4.339	0.9939	ATLAS

NOTE—This table is published in its entirety in the machine-readable format. A portion is shown here for guidance for regarding its form and content.

NOTE—Flag indicates if brightness measurement is the measured magnitude (flag = 1) or a 3σ upper limit (flag = 0).

initial brightening rate to the 3σ limiting magnitude from Hsieh et al. (2023) of 22.5 mag, which we assume to be the nuclear apparent magnitude of 2023 RN₃, we estimate the activity likely started within about 10 days of the first ZTF detection on 2023 August 26. Our observed brightness maximum, combined with the limiting magnitude measurement from Hsieh et al. (2023), would imply a total increase in brightness of $\Delta m > 5.4$ mag, comparable to that observed for the large cometary outbursts of the Centaur 29P/Schwassman-Wachmann 1 (Trigo-Rodríguez et al. 2008; Miles 2016; Lin 2023) and the comet 12P/Pons-Brooks (Manzini et al. 2023; Trigo-Rodríguez et al. 2024). From visual inspection of our reduced magnitude lightcurve, we do not see evidence of any secondary cometary outbursts by 2023 RN₃ with its brightness evolution consistent with a single sudden rise in brightness followed by a small decrease to a relatively constant magnitude. Our 3σ upper limits before 2023 August 26 preclude an epoch of cometary activity as bright as the observed 2023 epoch, however we cannot rule out lower-level cometary activity occurring before this date.

3.2. Color Evolution

We use the dual filter coverage of ATLAS, ZTF, and LOOK to search for any changes in 2023 RN₃’s $c - o$ or $g - r$ color across time. As per Section 3.1, for each magnitude measurement we use the geocentric and heliocentric distances of 2023 RN₃ at the time of observation to calculate the corresponding reduced magnitude. We apply the two methods used in Dobson et al. (2024) for measuring color evolution for a varying lightcurve.

The first method involves binning all the magnitude measurements from a given dataset by epoch of observation. ATLAS measurements that are separated in time by < 2 days (its approximate observation cadence) are counted as part of an epoch. For ZTF and LOOK, there are often both g and r observations on the same night, thus we consider magnitude measurements separated by < 0.5 days as part of one epoch. For each epoch, if observations in both filters are present, the mean reduced magnitude of each filter is calculated, and with its associated uncertainty calculated as the standard deviation of the magnitudes in each filter. The corresponding $c - o$ or $g - r$ color index of each is calculated by subtracting these mean magnitudes, with the associated uncertainties propagated in quadrature.

The second method involves fitting polynomial splines to the magnitude values of a given filter for a given survey, allowing us to account for any sudden change in 2023 RN₃’s brightness across time. To ensure well-constrained polynomial fits, we only fit ZTF g and r observations before MJD 60270 due to the scarcity of data in these filters

Table 3. Magnitude offsets for 2023 RN₃ apparent magnitudes in each filter, correcting to the ATLAS *o* filter.

Filter	Magnitude Offset (mag)
ATLAS <i>c</i>	-0.563
ATLAS <i>o</i>	0.000
PS1 <i>g</i> (ZTF)	-0.546
PS1 <i>r</i> (ZTF)	0.063
PS1 <i>w</i> (LOOK)	0.164
PS1 <i>g'</i> (LOOK)	-0.593
PS1 <i>r'</i> (LOOK)	-0.016
PS1 <i>i'</i> (LOOK)	0.097

after these dates. Our ATLAS *c* filter has too few measurements to sufficiently constrain the value this way, therefore we do not include it in our analysis. For each filter, we generate 10^3 datasets of synthetic magnitudes. We create a synthetic magnitude dataset by duplicating the measured magnitude values and adding to each magnitude value a random number generated from a Gaussian distribution centred on zero with a standard deviation equal to the measured magnitude’s uncertainty. We then fit a 3rd order polynomial spline to each set of synthetic magnitude values. For a given magnitude measurement in a given filter, we calculate 2023 RN₃’s magnitude in the other filter at the same time of measurement as predicted by its fitted spline. These two magnitude measurements are then used to calculate 2023 RN₃’s ($g - r$) color at that time. This method is repeated for each of the 10^3 synthetic datasets.

Figure 3 shows the resulting ZTF and LOOK color indices across time, calculated from binning data by epoch of observation. The ZTF and LOOK color indices calculated from the spline fitting method are shown in Figures 4 and 5, respectively. We see no significant change in color across our baseline of observation, with its $c - o$ and $g - r$ color indices remaining constant within uncertainties. The mean $c - o$ from ATLAS, calculated from spline fitting, is 0.316 ± 0.023 with a median of 0.317. From binning our observations by epoch of observation, the mean $g - r$ values from ZTF and LOOK are 0.559 ± 0.044 and 0.597 ± 0.029 in their respective filter systems, with medians of 0.553 and 0.556 respectively. When fitting our observations with splines, the mean $g - r$ values from ZTF and LOOK in their respective filter systems are 0.601 ± 0.023 and 0.592 ± 0.008 , with medians of 0.583 and 0.559 respectively. Our $g - r$ values for each filter system are consistent to $< 2\sigma$ for both methods, and are also consistent with the color measured by Hsieh et al. (2023), $g - r = 0.61 \pm 0.03$. For comparison, the corresponding solar color indices in these filter systems are $(c - o) = 0.29$ and $(g - r)_{PS1} = 0.39$ (Tonry et al. 2018a; Willmer 2018). Hence, assuming our data to be dominated by a coma as evidenced by both the comet’s fuzzy appearance in previous observations (Hsieh et al. 2023) and the large increase in the comet’s brightness, the color of 2023 RN₃’s coma is significantly redder than the Sun and similar to previously observed cometary dust comae (Solontoi et al. 2012).

3.3. Surface Brightness Evolution

The increased spatial resolution of the 2023 RN₃ observations from LOOK and Liverpool telescope (0.39 and 0.30 $''$ /pixel, respectively) compared to ATLAS and ZTF (1.86 and 1.01 $''$ /pixel, respectively) allow us to analyze the structure of 2023 RN₃’s PSF and investigate its evolution across time. We use our photometric detections of 2023 RN₃ where the comet’s SNR is ≥ 26 to enable accurate analysis of its radial profile. We utilize Source Extractor Python (Bertin & Arnouts 1996; Barbary 2016) to detect background field stars from the PanSTARRS Mean DR2 catalog (Chambers et al. 2016; Magnier et al. 2020; Flewelling et al. 2020) and select the stars which satisfy the following criteria: 1) they are isolated sources i.e. no other detected source lies within 10 arcsec of their centroid to prevent contamination; 2) the difference between their PanSTARRS Mean DR2 PSF magnitudes and Kron magnitudes in the *i* filter is less than 0.05 mag to separate stars from galaxies; and 3) their *g*-filter PanSTARRS Mean DR2 PSF magnitude is brighter than 20th mag to ensure they are of comparable brightness to 2023 RN₃. We then select the

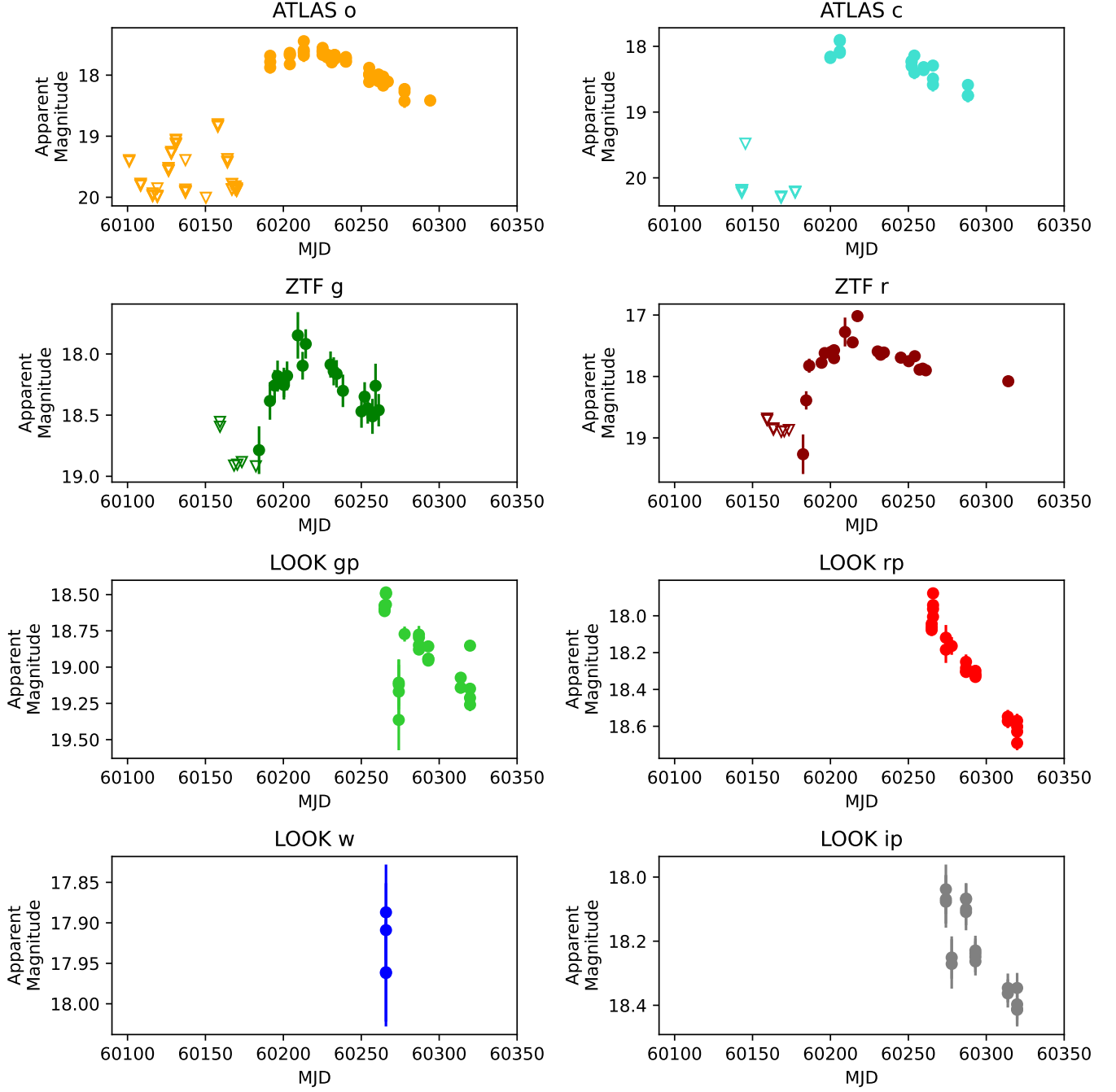


Figure 1. Lightcurve of 2023 RN₃ (apparent magnitude across time) in each filter. Filled circles indicate magnitude measurements, empty markers triangle indicate 3σ upper limits.

10 stars whose peak fluxes as measured with Source Extractor Python are closest to that of 2023 RN₃ to compare to the comet. We use the *RadialProfile* function of the *photutils* Python library (Bradley 2023) to measure the radial profile of 2023 RN₃ in comparison to the background stars, utilizing the background flux value calculated using the *Background* function from *Source Extractor Python* to remove the background noise contribution from each radial profile.

Figures 6 and 7 show respectively LOOK and Liverpool Telescope observations of 2023 RN₃ and for comparison a field star with similar peak flux, their corresponding contour plots, and the radial profile of 2023 RN₃ as compared to the 10 field stars of similar brightness, with the linear fit to the profile of 2023 RN₃ overplotted. We calculate the full

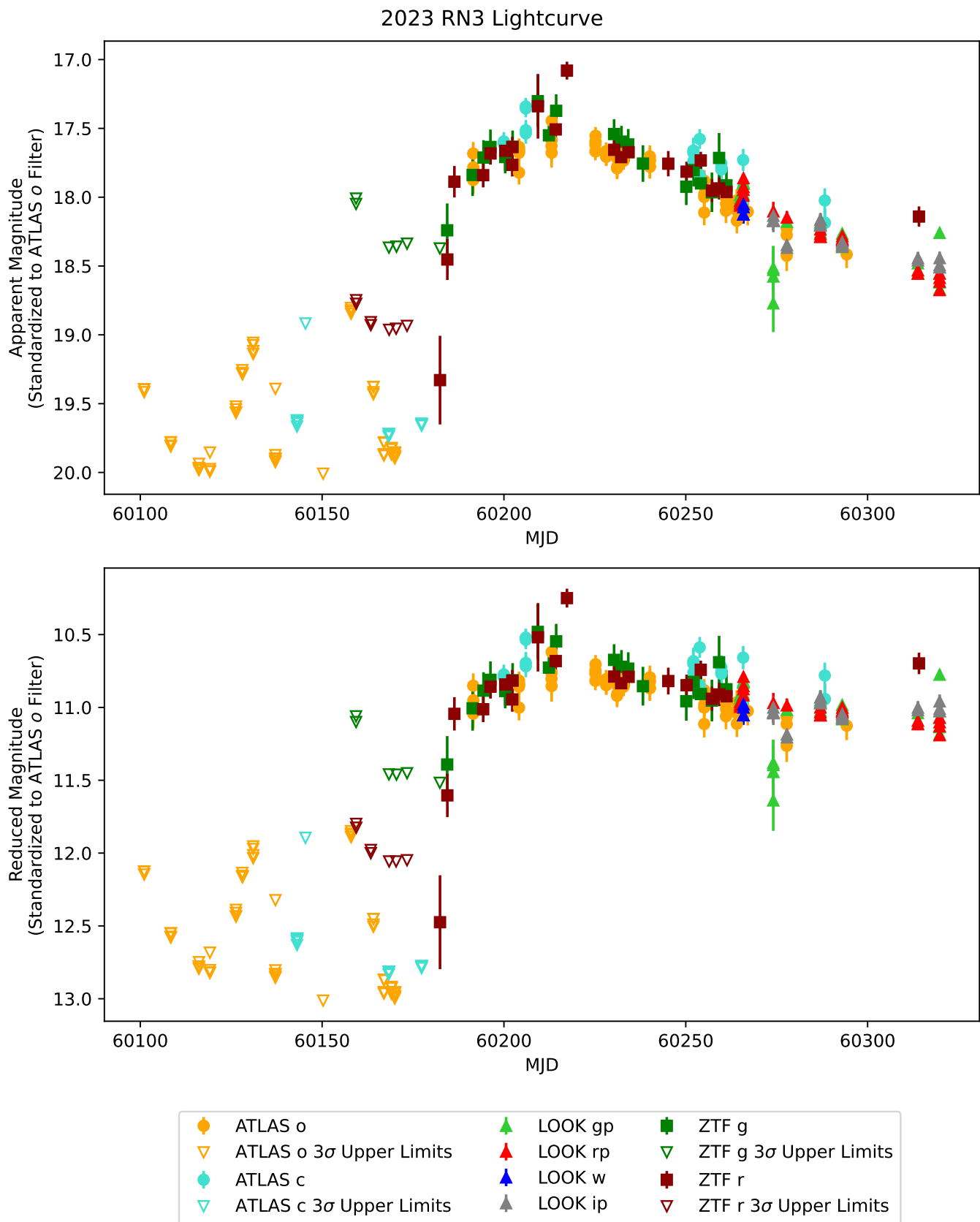


Figure 2. Lightcurve of 2023 RN₃ plotting apparent magnitude (top) and reduced magnitude (bottom) across time. All magnitudes are corrected to the ATLAS o filter wavelength. Filled markers indicate magnitude measurements of SNR ≥ 3 , empty markers indicate 3σ upper limits.

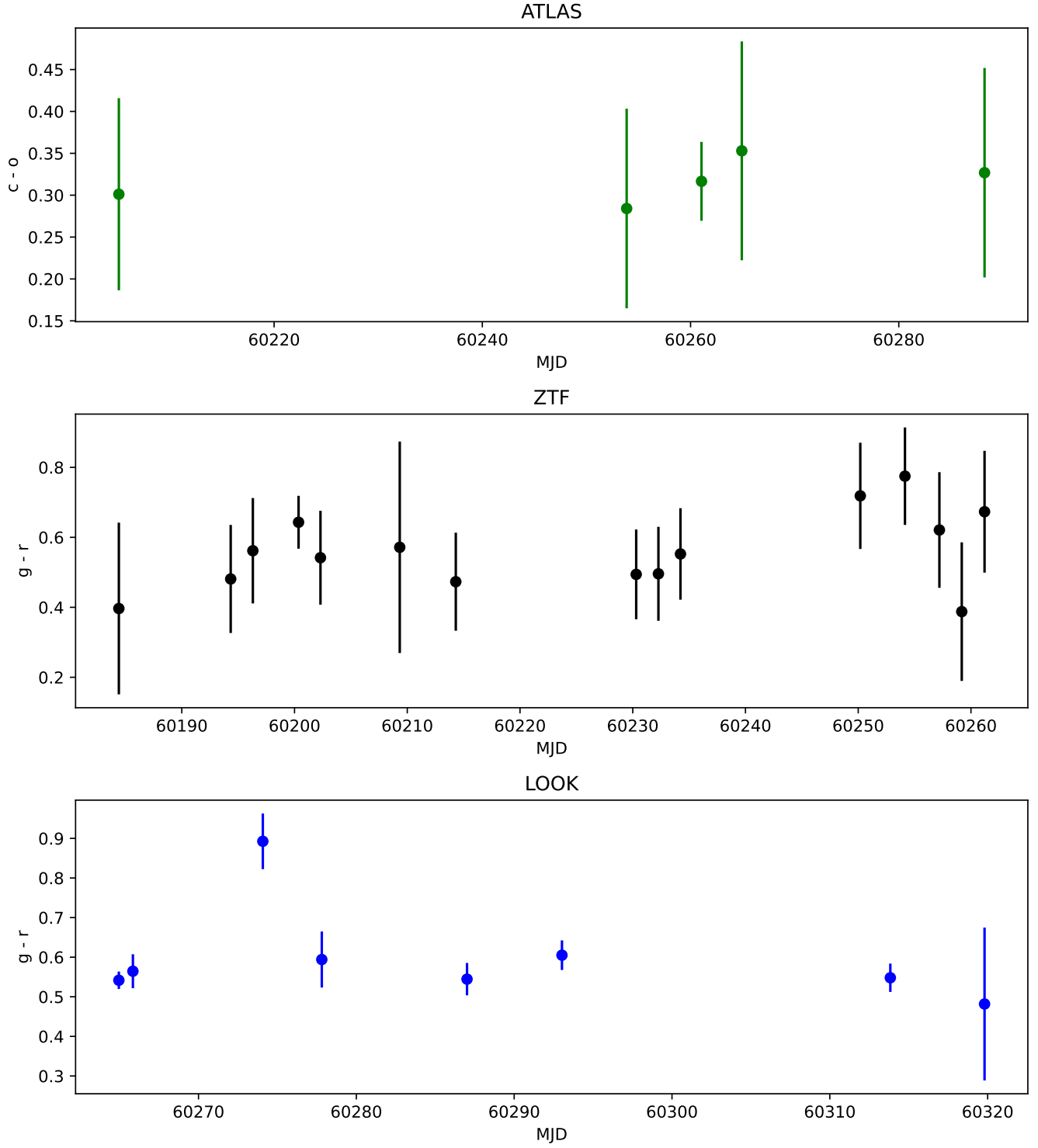


Figure 3. ATLAS $c - o$ (upper), ZTF $g - r$ (center), and LOOK $g - r$ (lower) color index values calculated from binning observations by epoch plotted across time.

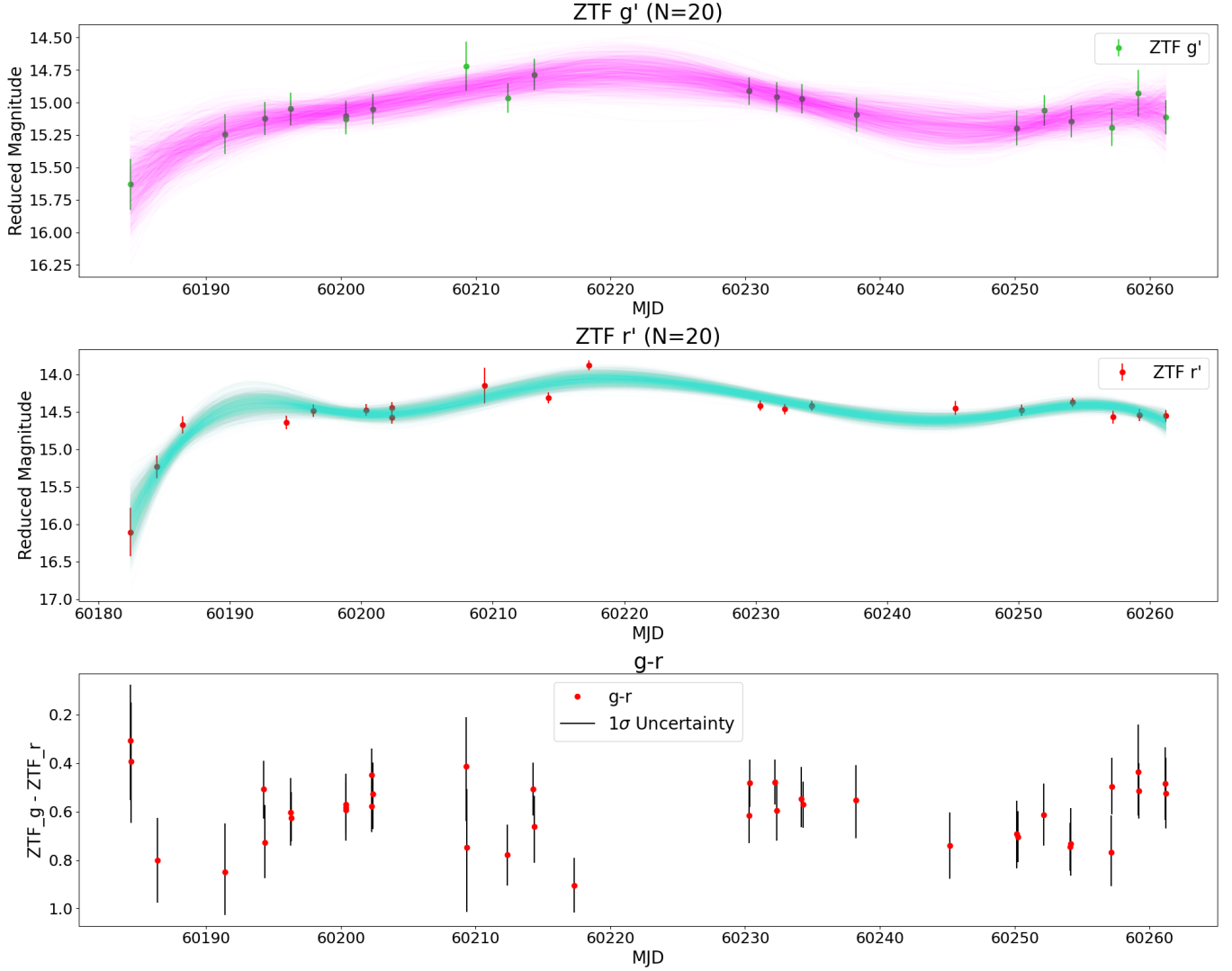


Figure 4. Top: ZTF g filter reduced magnitudes (green circles) vs. time with 3rd order interpolated splines fitted to synthetic data overplotted (green). Middle: ZTF r filter reduced magnitudes (red circles) vs. time with 3rd order interpolated splines fitted to synthetic data overplotted (turquoise). Bottom: $g - r$ color index value calculated from the predicted magnitudes in each filter from the synthetic magnitudes plotted across time. Red circles denote nominal color index values with green lines highlighting the range that includes the central 68.3% of synthetic values.

width half maximum (FWHM) of 2023 RN₃ and the comparison stars using the equation:

$$FWHM = 2\sqrt{\ln(2)(a^2 + b^2)} \quad (2)$$

where a and b are the semimajor and semiminor axes of the fitted PSF to a given source detected by Source Extractor Python. The FWHM of 2023 RN₃ and the mean FWHM of the 10 comparison stars for each LOOK and Liverpool Telescope observation are included in the caption of each corresponding figure in Figure Sets 1 and 2. We find that for each observation, the FWHM of 2023 RN₃ is extended compared to that of the background field stars and/or the radial profile of 2023 RN₃ deviates from the background star profile. This indicates the presence of a spatially extended coma, consistent with the findings of Hsieh et al. (2023).

3.4. $Af\rho$

To examine 2023 RN₃'s dust production rate, we use the parameter $Af\rho$, introduced by A'Hearn et al. (1984), which is proportional to the mass loss rate of an observed comet. The product of the cometary albedo A , dust grain filling factor f , and aperture radius ρ , $Af\rho$ can be calculated via:

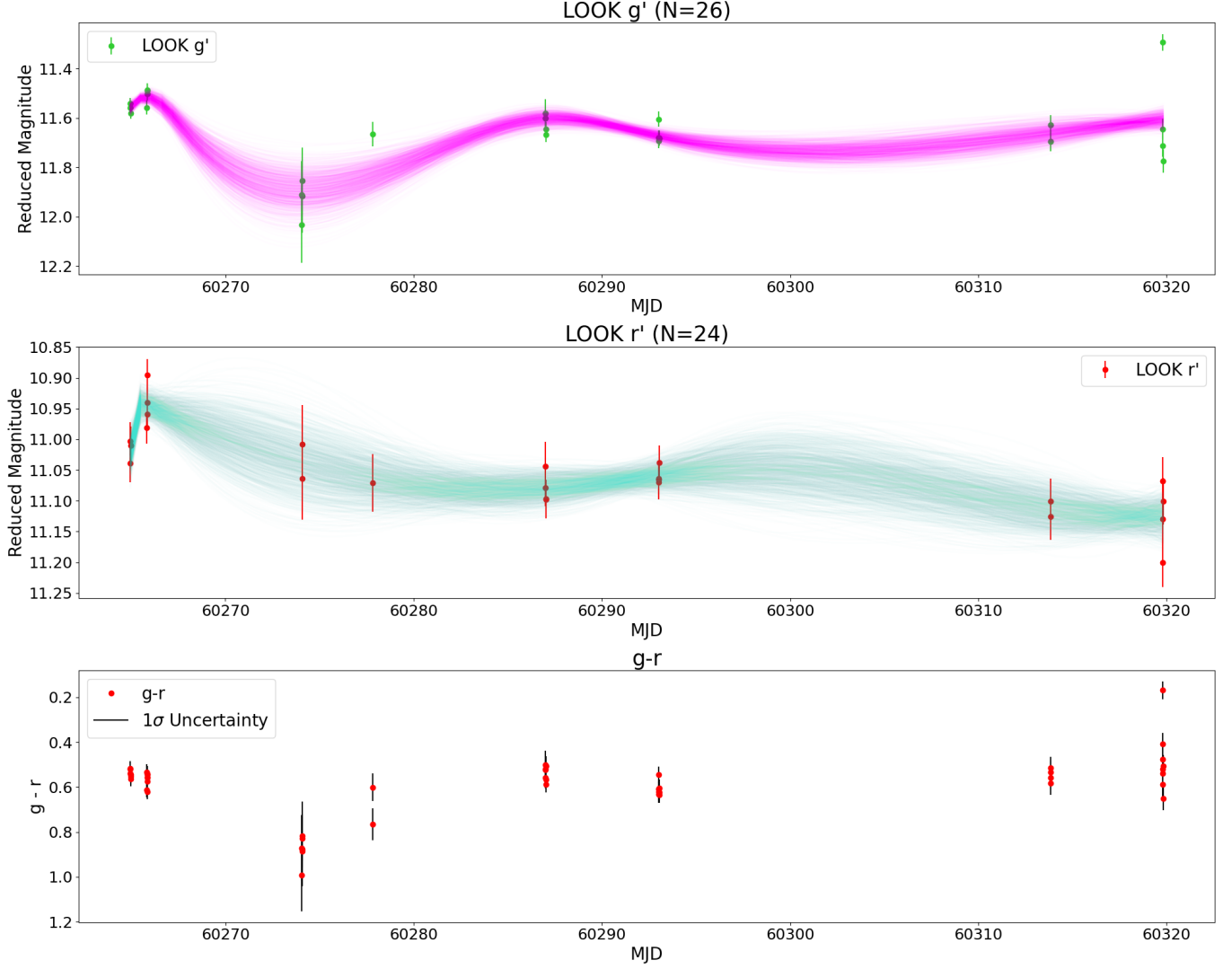


Figure 5. Top: LOOK g' filter reduced magnitudes (green circles) vs. time with 3rd order interpolated splines fitted to synthetic data overplotted (green). Middle: LOOK r' filter reduced magnitudes (red circles) vs. time with 3rd order interpolated splines fitted to synthetic data overplotted (turquoise). Bottom: $g - r$ color index value calculated from the predicted magnitudes in each filter from the synthetic magnitudes plotted across time. Red circles denote nominal color index values with green lines highlighting the range that includes the central 68.3% of synthetic values.

$$Af\rho = \frac{4R_H^2\Delta^2}{\rho} \frac{F_{com}}{F_{Sun}} \quad (3)$$

where Δ is the geocentric distance of an observed comet (measured in centimetres), R_H is its heliocentric distance (measured in au), ρ the aperture radius used to measure its brightness (measured in cm), F_{com} is the measured flux of the comet, and F_{Sun} is the solar flux measured at 1 au. This equation can be alternatively expressed in terms of the magnitudes of the comet M_{com} and Sun M_{Sun} as:

$$Af\rho = \frac{4R_H^2\Delta^2}{\rho} 10^{0.4(M_{Sun}-M_{com})} \quad (4)$$

We use an aperture radius of $\rho = 20,000$ km as per Section 3.1, and the same geocentric and heliocentric distances as used in Section 3.2. The cometary activity levels exhibited by 2023 RN₃ are wavelength dependent, as the color of the material emitted by the comet relative to the Sun will have a corresponding effect on the measured $Af\rho$ values.

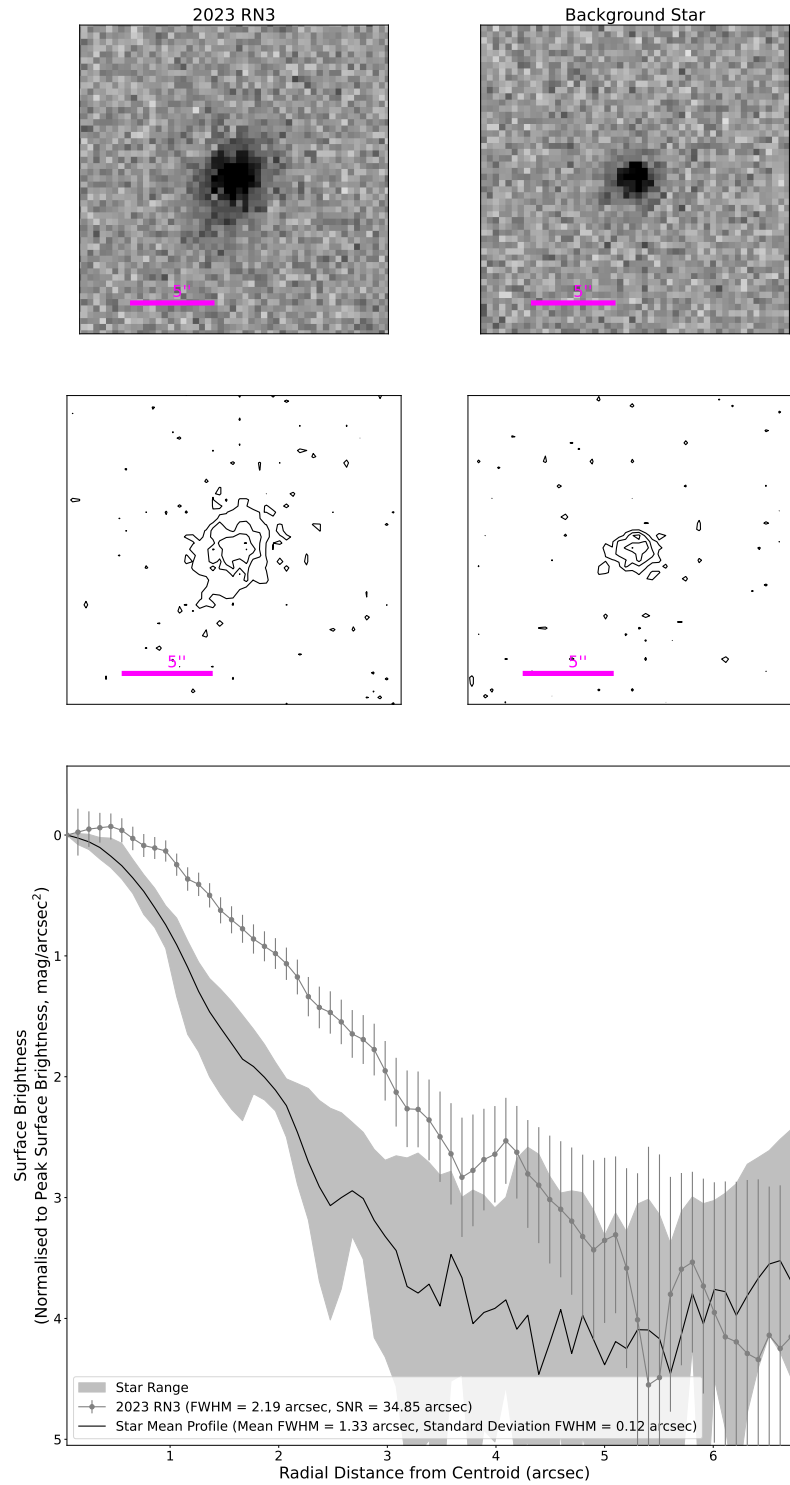


Figure 6. Top row: 2024 January 04 (MJD 60313.8750614) i-filter LOOK observation of 2023 RN₃ (left) and a nearby background star (right). Center row: Corresponding contour plots of the PSFs of 2023 RN₃ (left) and the same background star (right). Bottom: Radial profile of 2023 RN₃ (grey circles) compared to mean radial profile (black line) and range of profiles (grey shaded) of 10 nearby field stars from 2024 January 04 i-filter LOOK observation, plotting instrumental surface brightness (in units of magnitudes/arcsec²) normalised to the peak brightness of 2023 RN₃ vs. radial distance from the PSF centroid. Note: this figure comprises part of a figure set which can be found in the online published version of this paper.

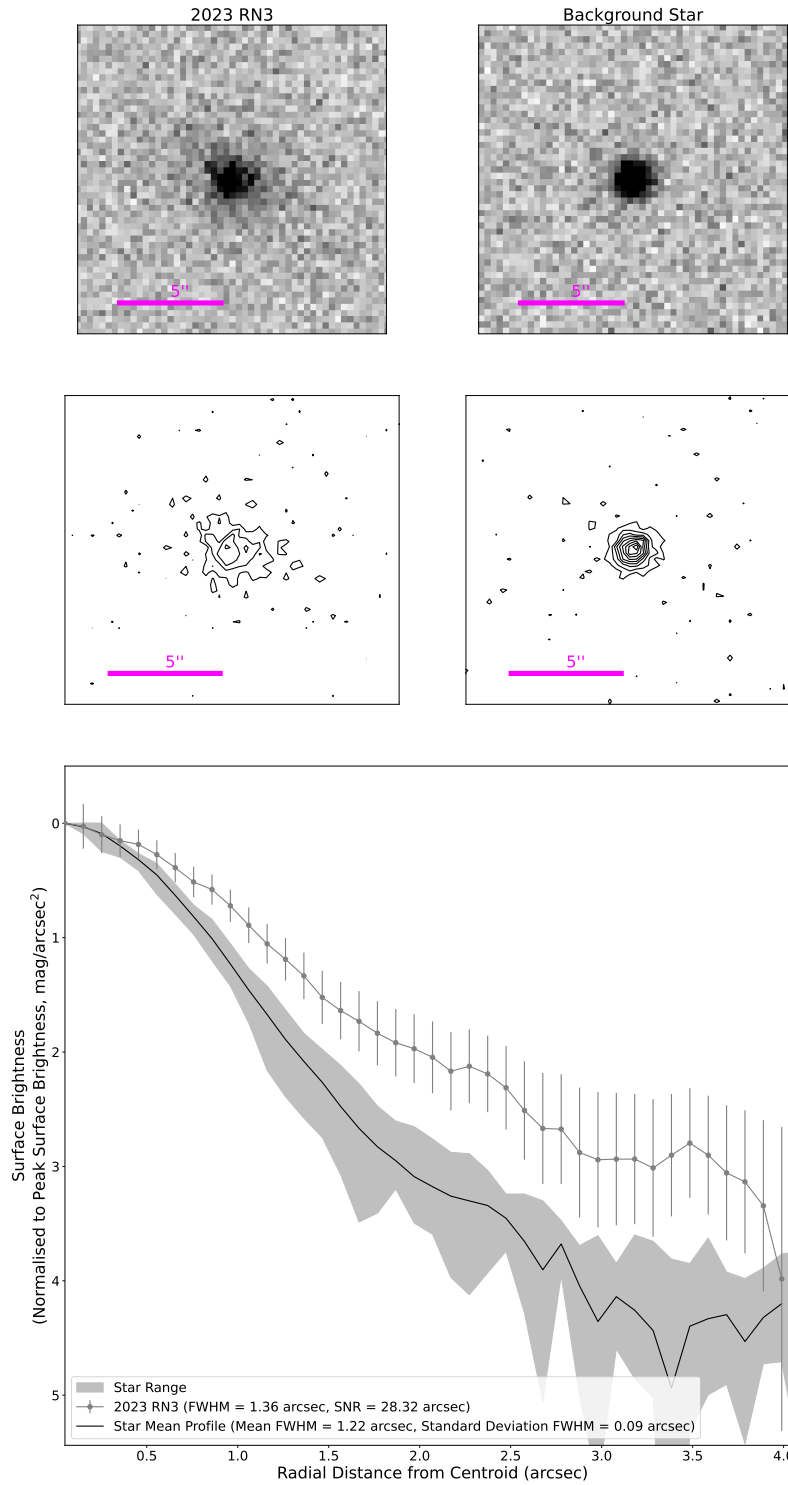


Figure 7. Top row: 2023 December 14 (MJD 60292.826273) SDSS-I filter Liverpool Telescope observation of 2023 RN₃ (left) and a nearby background star (right). Center row: Corresponding contour plots of the PSFs of 2023 RN₃ (left) and the same background star (right). Bottom: Radial profile of 2023 RN₃ (grey circles) compared to mean radial profile (black line) and range of profiles (grey shaded) of 10 nearby field stars from 2023 December 14 SDSS-I filter LOOK observation, plotting instrumental surface brightness (in units of magnitudes/arcsec²) normalised to the peak brightness of 2023 RN₃ vs. radial distance from the PSF centroid. Note: this figure comprises part of a figure set which can be found in the online published version of this paper.

As 2023 RN₃ has not undergone any significant color evolution across our dataset, we take our lightcurve corrected to the ATLAS *o* filter from Figure 2 in Section 3.1 to calculate $Af\rho$. For this calculation, we apply the ATLAS *o* filter solar magnitude measurement of -26.982 (Gillan et al. 2024). $Af\rho$ is also dependent on the solar phase angle of the comet at the time of measurement due to the light-scattering properties of the coma dust particles. We correct our $Af\rho$ values for effects of phase angle using the Schleicher-Marcus² cometary phase function (Schleicher et al. 1998; Marcus 2007; Schleicher 2010).

The resulting phase-corrected values, $A(0^\circ)f\rho$, are plotted across time in Figure 8, showing 2023 RN₃ to rapidly increase in activity before plateauing around a maximum $A(0^\circ)f\rho$ value of approximately 400 cm for most of our observations. This is consistent with continuous and sustained activity instead of a brief outburst. We consider the continuous nature of 2023 RN₃'s cometary activity sufficient to permit comparison of its $Af\rho$ value to other objects. 2023 RN₃'s maximum $A(0^\circ)f\rho$ value is greater than that of most JFCs (Shubina et al. 2023; Gillan et al. 2024; Kareta et al. 2024) yet is far less than those of outbursts exhibited by the JFC 17P/Holmes (Trigo-Rodríguez et al. 2008; Lin et al. 2009; Trigo-Rodríguez et al. 2010) and the Centaur 29P Schwassman-Wachmann 1 (Trigo-Rodríguez et al. 2010; Lin 2023), which increased the apparent brightness of the respective objects by several magnitudes, and whose maximum $Af\rho$ values were of the order of $10^3 - 10^5$ cm. This difference in $Af\rho$ values may be due to different sizes or numbers of active regions on the objects' surfaces, though a comparison of such active regions is beyond the scope of this paper.

3.5. Orbital Evolution

As mentioned above, Lilly et al. (2024) found evidence that cometary activity in Centaurs and high-perihelion JFCs may be triggered by rapid changes in semi-major axis due to planetary perturbations. To investigate this possibility for 2023 RN₃, we performed an N-body simulation using *REBOUND* (Rein & Liu 2012) and *astropy* (Astropy Collaboration et al. 2013, 2018, 2022). We obtained the most recent orbital elements with epoch JD 2460222.5 \equiv 2023.759 TDB from the JPL solar system Database via the JPL SSDB API, calculated from observations up to 13 January 2024, and generated an additional 100 clones using the associated covariance matrix. Including the 8 major planets, we integrated all bodies for ± 500 years from the orbital epoch using the IAS15 integrator (Rein & Spiegel 2015). The resulting orbital evolution of all 101 test objects are shown in Figure 9. We found that the orbit of 2023 RN₃ is well constrained between the years 1549 and 2388. Planetary encounters on those dates significantly increase orbital uncertainties outside this date range. At the current epoch, 2023 RN₃ has just experienced a rapid increase in semi-major axis of $\Delta a = +0.3$ au due to a distant encounter with Jupiter, with a small simultaneous increase in eccentricity e maintaining the same perihelion distance q . We note that Lilly et al. (2024) found almost all activity in Centaurs correlated with rapid *decreases* in a , with only 4 out of 56 objects having undergone increases in a . The most similar object in their study was C/2013 P4 (Pan-STARRS), which also underwent $\Delta a = +0.3$ au 176 years ago, although of course we have no information on its activity at that time. Hence it is unclear whether this small 3% increase in a would or could lead to the sudden onset of significant activity observed by us in 2023 RN₃.

4. SUMMARY AND CONCLUSIONS

We analyzed the 2023 cometary activity of the JFC 2023 RN₃ using serendipitous observations from the ATLAS and ZTF surveys combined with targeted follow-up observations from LOOK and the Liverpool Telescope. This resulted in a lightcurve spanning seven months of high-cadence observations. We used this lightcurve of 2023 RN₃ to analyze its evolution in brightness, color index, and activity levels. We also utilized our higher-resolution observations from LOOK and the Liverpool Telescope to analyze the radial profile of 2023 RN₃. Our key findings are:

- The lightcurve of 2023 RN₃ is indicative of the onset of an epoch of continuous cometary activity, commencing about 10 days before its first detection on 2023 August 26, and reaching a maximum brightness of about 17.5 mag, corresponding to a brightness increase of ≥ 5.4 mag based on upper limits from Hsieh et al. (2023).
- We do not observe any significant change in color across our observations.
- Analysis of 2023 RN₃'s surface brightness radial profile shows significant extension compared to background stars, indicating the presence of a spatially-extended coma, consistent with Hsieh et al. (2023).

² <https://asteroid.lowell.edu/comet/dustphase/details>

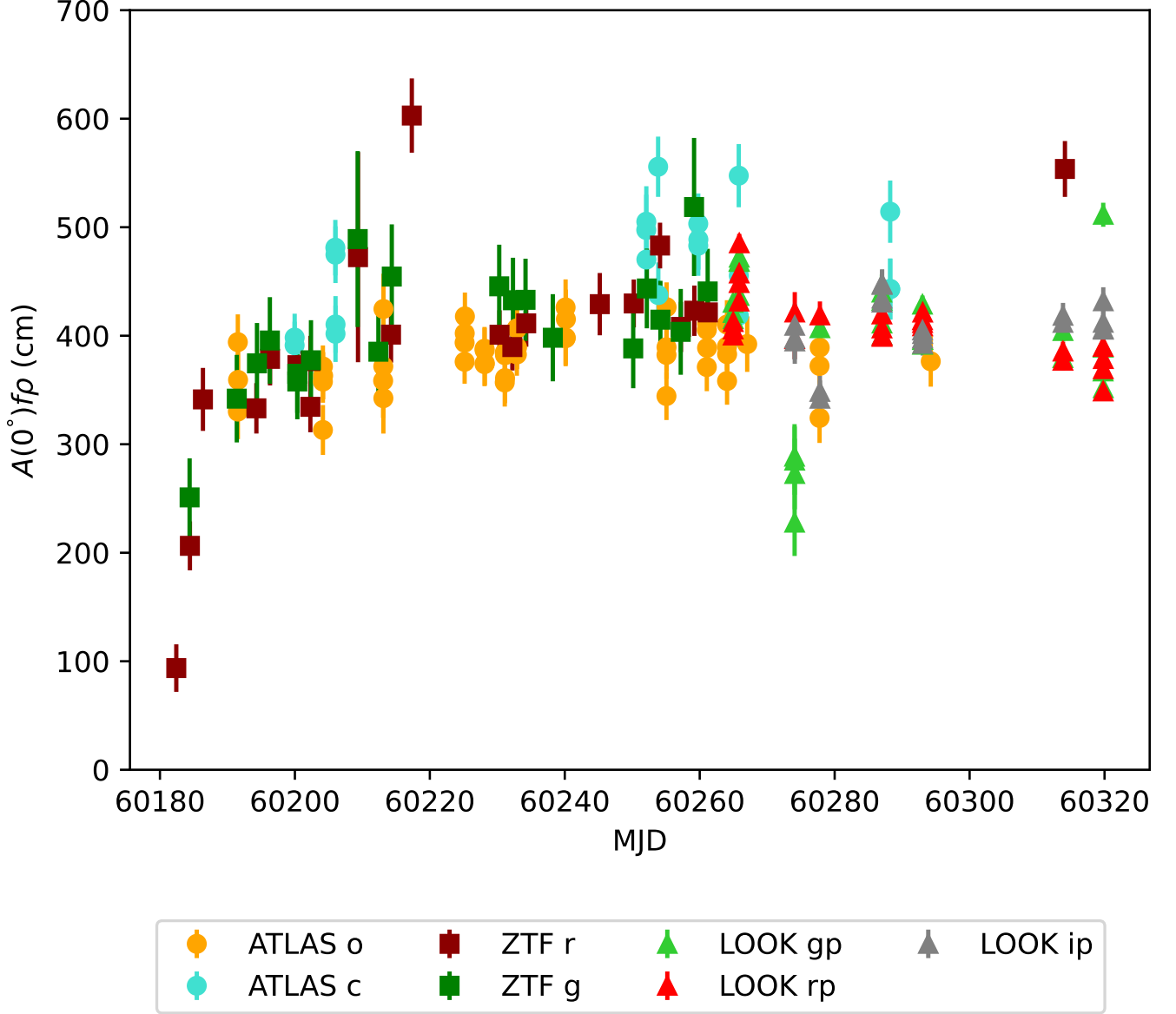


Figure 8. $A(0^\circ)f\rho$ values of 2023 RN₃ across time. $A(0^\circ)f\rho$ values have been corrected for color and phase effects.

- We measure a maximum dust production rate of $A(0^\circ)f\rho \sim 400$ cm, larger than that of most JFCs, but smaller than that observed for the outbursts of 29P and 17P.
- We find that 2023 RN₃ has experienced an increase in semimajor axis of $a = +0.3$ au due to a planetary encounter with Jupiter, coinciding with its current active epoch.

With a heliocentric distance at the time of its detected onset of cometary activity of 5.301 au, 2023 RN₃ resides beyond the so-called ‘ice line’ at ~ 3 au, interior to which direct sublimation of water ice is the dominant mechanism for observed cometary activity (Meech & Svoren 2004; Womack et al. 2017). This rules out direct sublimation of water-ice as the mechanism behind 2023 RN₃’s 2023 cometary activity. Possible drivers of this cometary activity could be the volatile species of CO or CO₂ which are thought to dominate observed cometary activity beyond the ‘ice line’ (A’Hearn et al. 2012; Ootsubo et al. 2012; Reach et al. 2013; Cochran et al. 2015; Bauer et al. 2015; Womack et al. 2017). While we have shown that 2023 RN₃ has recently experienced a slight increase in semimajor axis due to a planetary encounter, whether this has led to the observed onset of cometary activity remains ambiguous as cometary

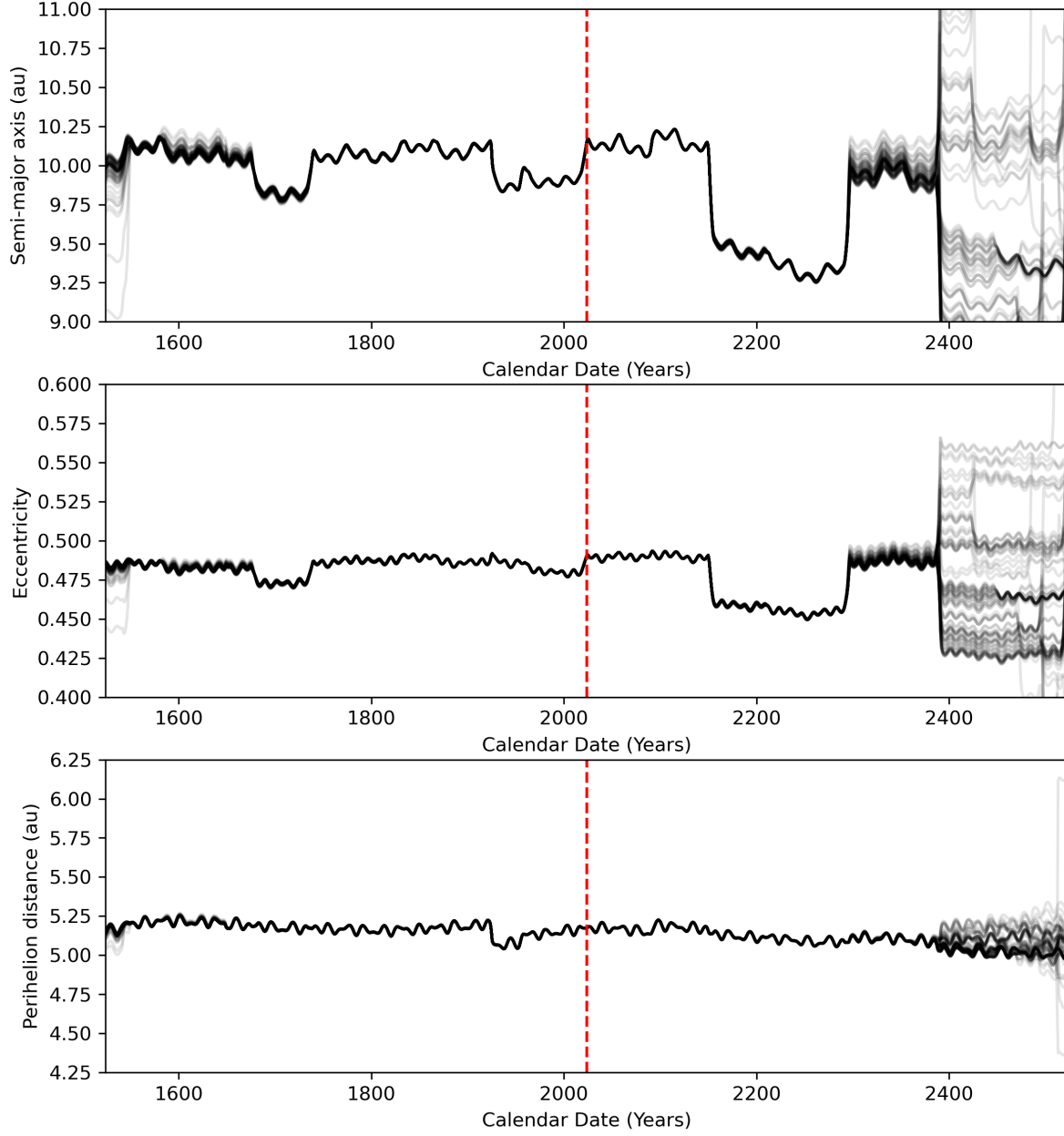


Figure 9. Orbital evolution calculations of the 2023RN₃ nominal orbit and 100 clones. Top plot; semi-major axis a versus date. The red dashed line indicates the starting epoch of the orbital integrations. The y-axis range of the top plot has been chosen to clearly show the small jumps in a near the current epoch. Middle and bottom plots; as for the top plot but showing eccentricity e and perihelion distance q .

activity in Centaurs and JFCs triggered by planetary encounters is normally associated with rapid decreases in the objects' semimajor axes (Lilly et al. 2024). The lack of any detected periodic outbursts by 2023 RN₃ may be due to its nucleus having a bilobate structure akin to that of 29P/Schwassman-Wachmann 1 (Faggi et al. 2024), shielding a possible patch of volatiles from direct insolation until the onset of its recent active epoch. Confirmation of the nuclear shape of 2023 RN₃ via lightcurve analysis or direct imaging could help test this theory.

Estimates of the maximum dust-production levels across 2023 RN₃'s 2023 cometary activity are considerably smaller than those of cometary outbursts with similar changes in brightness. 2023 RN₃'s $Af\rho$ maximum is consistent with the JFC population as a whole (Shubina et al. 2023; Gillan et al. 2024; Kareta et al. 2024), albeit at the high end of the distribution, and is also consistent with those exhibited by the Centaur population (ranging from $\sim 10^2 - 10^5$ cm). This further highlights 2023 RN₃'s relevance to the study of cometary activity in both these populations.

We highlight that this object, and its corresponding cometary activity, was detected via serendipitous observations from ATLAS. The upcoming Legacy Survey of Space and Time by the Vera C. Rubin Observatory (LSST Science Collaboration et al. 2009; Jurić et al. 2019; Ivezić et al. 2019; Schwamb et al. 2023), with its high observation cadence and faint limiting magnitude, will allow us to track the continued brightness evolution of 2023 RN₃ and detect any changes in activity such as future cometary outbursts. LSST's faint limiting magnitude of ~ 24 mag (Bianco et al. 2022) will allow us to discover many more such instances of cometary activity across the solar system, helping us to further shed light on the evolution of short period comets.

5. ACKNOWLEDGEMENTS

MMD was supported by the UK Science Technology Facilities Council (STFC) grant ST/V506990/1. MES was supported by the UK Science Technology Facilities Council (STFC) grant ST/X001253/1. AF was supported by UK STFC grant ST/X001253/1. MSK was supported by the NASA solar system Observations program (80NSSC20K0673). LJS acknowledges support by the European Research Council (ERC) under the European Union's Horizon 2020 research and innovation program (ERC Advanced Grant KILONOVA No. 885281). JM acknowledges support from the Department for the Economy (DfE) Northern Ireland postgraduate studentship scheme. This research has made use of data and/or services provided by the International Astronomical Union's Minor Planet Center. This research has made use of services provided by NASA's Astrophysics Data System. This work has made use of data and services provided by the Horizons system of the Jet Propulsion Laboratory.

This work has made use of data from the Asteroid Terrestrial-impact Last Alert System (ATLAS) project. The Asteroid Terrestrial-impact Last Alert System (ATLAS) project is primarily funded to search for near earth asteroids through NASA grants NN12AR55G, 80NSSC18K0284, and 80NSSC18K1575; byproducts of the NEO search include images and catalogs from the survey area. This work was partially funded by Kepler/K2 grant J1944/80NSSC19K0112 and HST GO-15889, and STFC grants ST/T000198/1 and ST/S006109/1. The ATLAS science products have been made possible through the contributions of the University of Hawaii Institute for Astronomy, the Queen's University Belfast, the Space Telescope Science Institute, the South African Astronomical Observatory, and The Millennium Institute of Astrophysics (MAS), Chile.

This work is based on observations obtained with the Samuel Oschin Telescope 48 inch Telescope at the Palomar Observatory as part of the Zwicky Transient Facility project. Major funding has been provided by the U.S. National Science Foundation under grant No. AST-1440341 and by the ZTF partner institutions: the California Institute of Technology, the Oskar Klein Centre, the Weizmann Institute of Science, the University of Maryland, the University of Washington, Deutsches Elektronen-Synchrotron, the University of Wisconsin-Milwaukee, and the TANGO Program of the University System of Taiwan.

This work makes use of observations from the Las Cumbres Observatory global telescope network. Observations with the LCOGT 1m were obtained as part of the LCO Outbursting Objects Key (LOOK) Project (KEY2020B-009).

This work has utilized observations from the Liverpool Telescope. The Liverpool Telescope is operated on the island of La Palma by Liverpool John Moores University in the Spanish Observatorio del Roque de los Muchachos of the Instituto de Astrofísica de Canarias with financial support from the UK Science and Technology Facilities Council.

Data Access: All photometric data used in this study is provided in full as supplementary information accompanying this paper. Raw and Calibrated Observations from Las Cumbres Observatory used in this study are available at the LCO Science Archive (<https://archive.lco.global>; proposal code KEY2020B-009) after an embargo/proprietary period

of 12 months. Calibrated observations from the Liverpool Telescope used in this study are available at the Liverpool Telescope Data Archive (https://telescope.ljmu.ac.uk/cgi-bin/lt_search; observing program XPQ23B01) after a proprietary period of one year after the end of the observing semester when the observations were acquired (observing semester 2023B).

Facilities: ATLAS (Chile, Haleakala, Mauna Loa, and South Africa telescopes), PO:1.2m (ZTF), LCOGT (1-m telescopes), Liverpool:2m

Software: Astropy (Astropy Collaboration et al. 2013, 2018, 2022), BANZAI (McCully et al. 2018), CALVIACAT (Kelley & Lister 2021), IAS15 (Rein & Spiegel 2015), Jupyter Notebook (Kluyver et al. 2016), math (Van Rossum 2020), Matplotlib (Hunter 2007), NEOExchange (Lister et al. 2021), Numpy (van der Walt et al. 2011; Harris et al. 2020), os (Van Rossum 2020), Pandas (pandas development team 2020), Photutils (Bradley 2023), python (<https://www.python.org>), REBOUND (Rein & Liu 2012), SAOImageDS9 (Joye 2019), SciPy (Virtanen et al. 2020), Source Extractor Python (Bertin & Arnouts 1996; Barbary 2016)

REFERENCES

- A’Hearn, M. F., Schleicher, D. G., Millis, R. L., Feldman, P. D., & Thompson, D. T. 1984, *AJ*, 89, 579, doi: [10.1086/113552](https://doi.org/10.1086/113552)
- A’Hearn, M. F., Feaga, L. M., Keller, H. U., et al. 2012, *ApJ*, 758, 29, doi: [10.1088/0004-637X/758/1/29](https://doi.org/10.1088/0004-637X/758/1/29)
- Astropy Collaboration, Robitaille, T. P., Tollerud, E. J., et al. 2013, *A&A*, 558, A33, doi: [10.1051/0004-6361/201322068](https://doi.org/10.1051/0004-6361/201322068)
- Astropy Collaboration, Price-Whelan, A. M., Sipőcz, B. M., et al. 2018, *AJ*, 156, 123, doi: [10.3847/1538-3881/aabc4f](https://doi.org/10.3847/1538-3881/aabc4f)
- Astropy Collaboration, Price-Whelan, A. M., Lim, P. L., et al. 2022, *ApJ*, 935, 167, doi: [10.3847/1538-4357/ac7c74](https://doi.org/10.3847/1538-4357/ac7c74)
- Barbary, K. 2016, *The Journal of Open Source Software*, 1, 58, doi: [10.21105/joss.00058](https://doi.org/10.21105/joss.00058)
- Barnsley, R. M., Jermak, H. E., Steele, I. A., et al. 2016, *Journal of Astronomical Telescopes, Instruments, and Systems*, 2, 015002, doi: [10.1117/1.JATIS.2.1.015002](https://doi.org/10.1117/1.JATIS.2.1.015002)
- Bauer, J. M., Grav, T., Blauvelt, E., et al. 2013, *ApJ*, 773, 22, doi: [10.1088/0004-637X/773/1/22](https://doi.org/10.1088/0004-637X/773/1/22)
- Bauer, J. M., Stevenson, R., Kramer, E., et al. 2015, *ApJ*, 814, 85, doi: [10.1088/0004-637X/814/2/85](https://doi.org/10.1088/0004-637X/814/2/85)
- Bellm, E. C., Kulkarni, S. R., Graham, M. J., et al. 2019, *PASP*, 131, 018002, doi: [10.1088/1538-3873/aaecbe](https://doi.org/10.1088/1538-3873/aaecbe)
- Bertin, E., & Arnouts, S. 1996, *A&AS*, 117, 393, doi: [10.1051/aas:1996164](https://doi.org/10.1051/aas:1996164)
- Bianco, F. B., Ivezić, Ž., Jones, R. L., et al. 2022, *ApJS*, 258, 1, doi: [10.3847/1538-4365/ac3e72](https://doi.org/10.3847/1538-4365/ac3e72)
- Bradley, L. 2023, *astropy/photutils: 1.8.0*, 1.8.0, Zenodo, doi: [10.5281/zenodo.7946442](https://doi.org/10.5281/zenodo.7946442)
- Brown, T. M., Baliber, N., Bianco, F. B., et al. 2013, *PASP*, 125, 1031, doi: [10.1086/673168](https://doi.org/10.1086/673168)
- Chambers, K. C., Magnier, E. A., Metcalfe, N., et al. 2016, *arXiv e-prints*, arXiv:1612.05560, doi: [10.48550/arXiv.1612.05560](https://doi.org/10.48550/arXiv.1612.05560)
- Cochran, A. L., Levasseur-Regourd, A.-C., Cordiner, M., et al. 2015, *SSRv*, 197, 9, doi: [10.1007/s11214-015-0183-6](https://doi.org/10.1007/s11214-015-0183-6)
- Dobson, M. M., Schwamb, M. E., Fitzsimmons, A., et al. 2024, *PSJ*, 5, 165, doi: [10.3847/PSJ/ad543c](https://doi.org/10.3847/PSJ/ad543c)
- Faggi, S., Villanueva, G. L., McKay, A., et al. 2024, *Nature Astronomy*, doi: [10.1038/s41550-024-02319-3](https://doi.org/10.1038/s41550-024-02319-3)
- Fernández, J. A., Helal, M., & Gallardo, T. 2018, *Planet. Space Sci.*, 158, 6, doi: [10.1016/j.pss.2018.05.013](https://doi.org/10.1016/j.pss.2018.05.013)
- Flewelling, H. A., Magnier, E. A., Chambers, K. C., et al. 2020, *ApJS*, 251, 7, doi: [10.3847/1538-4365/abb82d](https://doi.org/10.3847/1538-4365/abb82d)
- Gillan, A. F., Fitzsimmons, A., Denneau, L., et al. 2024, *PSJ*, 5, 25, doi: [10.3847/PSJ/ad1394](https://doi.org/10.3847/PSJ/ad1394)
- Gladman, B., Marsden, B. G., & Vanlaerhoven, C. 2008, *Nomenclature in the Outer Solar System*, ed. M. A. Barucci, H. Boehnhardt, D. P. Cruikshank, A. Morbidelli, & R. Dotson, 43
- Graham, M. J., Kulkarni, S. R., Bellm, E. C., et al. 2019, *PASP*, 131, 078001, doi: [10.1088/1538-3873/ab006c](https://doi.org/10.1088/1538-3873/ab006c)
- Green, D. W. E. 2023, *COMET C/2023 RN3 (ATLAS)*
- Harris, C. R., Millman, K. J., van der Walt, S. J., et al. 2020, *Nature*, 585, 357, doi: [10.1038/s41586-020-2649-2](https://doi.org/10.1038/s41586-020-2649-2)
- Hsieh, H. H., Kelley, M. S. P., Lister, T. A., et al. 2023, *Research Notes of the American Astronomical Society*, 7, 263, doi: [10.3847/2515-5172/ad12ce](https://doi.org/10.3847/2515-5172/ad12ce)
- Hughes, D. W. 1990, *QJRAS*, 31, 69
- Hunter, J. D. 2007, *Computing in Science & Engineering*, 9, 90, doi: [10.1109/MCSE.2007.55](https://doi.org/10.1109/MCSE.2007.55)
- Ivezić, Ž., Kahn, S. M., Tyson, J. A., et al. 2019, *ApJ*, 873, 111, doi: [10.3847/1538-4357/ab042c](https://doi.org/10.3847/1538-4357/ab042c)
- Jewitt, D. 2009, *AJ*, 137, 4296, doi: [10.1088/0004-6256/137/5/4296](https://doi.org/10.1088/0004-6256/137/5/4296)
- Jewitt, D., & Hsieh, H. H. 2022, *arXiv e-prints*, arXiv:2203.01397, doi: [10.48550/arXiv.2203.01397](https://doi.org/10.48550/arXiv.2203.01397)
- Joye, W. 2019, *SAOImageDS9/SAOImageDS9 v8.0.1*, v8.0.1, Zenodo, Zenodo, doi: [10.5281/zenodo.2530958](https://doi.org/10.5281/zenodo.2530958)

- Jurić, M., Jones, R. L., Bryce Kalmbach, J., et al. 2019, arXiv e-prints, arXiv:1901.08549.
<https://arxiv.org/abs/1901.08549>
- Kareta, T., Noonan, J. W., Volk, K., Strauss, R. H., & Trilling, D. 2024, arXiv e-prints, arXiv:2404.08618, doi: [10.48550/arXiv.2404.08618](https://doi.org/10.48550/arXiv.2404.08618)
- Kelley, M., & Lister, T. 2021, mkelley/calviacat: v1.2.0, v1.2.0, Zenodo, doi: [10.5281/zenodo.5061298](https://doi.org/10.5281/zenodo.5061298)
- Kelley, M. S., & Wooden, D. H. 2009, Planet. Space Sci., 57, 1133, doi: [10.1016/j.pss.2008.11.017](https://doi.org/10.1016/j.pss.2008.11.017)
- Kluyver, T., Ragan-Kelley, B., Pérez, F., et al. 2016, in Positioning and Power in Academic Publishing: Players, Agents and Agendas, ed. F. Loizides & B. Schmidt (IOS Press), 87–90. <https://eprints.soton.ac.uk/403913/>
- Lilly, E., Hsieh, H., Bauer, J., et al. 2021, PSJ, 2, 155, doi: [10.3847/PSJ/ac139e](https://doi.org/10.3847/PSJ/ac139e)
- Lilly, E., Jevčák, P., Schambeau, C., et al. 2024, ApJL, 960, L8, doi: [10.3847/2041-8213/ad1606](https://doi.org/10.3847/2041-8213/ad1606)
- Lin, Z.-Y. 2023, PASJ, 75, 462, doi: [10.1093/pasj/psad012](https://doi.org/10.1093/pasj/psad012)
- Lin, Z.-Y., Lin, C.-S., Ip, W.-H., & Lara, L. M. 2009, AJ, 138, 625, doi: [10.1088/0004-6256/138/2/625](https://doi.org/10.1088/0004-6256/138/2/625)
- Lister, T., Kelley, M. S. P., Holt, C. E., et al. 2022, PSJ, 3, 173, doi: [10.3847/PSJ/ac7a31](https://doi.org/10.3847/PSJ/ac7a31)
- Lister, T. A., Gomez, E., Chatelain, J., et al. 2021, Icarus, 364, 114387, doi: [10.1016/j.icarus.2021.114387](https://doi.org/10.1016/j.icarus.2021.114387)
- LSST Science Collaboration, Abell, P. A., Allison, J., et al. 2009, arXiv e-prints, arXiv:0912.0201.
<https://arxiv.org/abs/0912.0201>
- Magnier, E. A., Chambers, K. C., Flewelling, H. A., et al. 2020, ApJS, 251, 3, doi: [10.3847/1538-4365/abb829](https://doi.org/10.3847/1538-4365/abb829)
- Manzini, F., Oldani, V., Ochner, P., Bedin, L. R., & Reguitti, A. 2023, The Astronomer's Telegram, 16194, 1
- Marcus, J. N. 2007, International Comet Quarterly, 29, 39
- Masci, F. J., Laher, R. R., Rusholme, B., et al. 2019, PASP, 131, 018003, doi: [10.1088/1538-3873/aae8ac](https://doi.org/10.1088/1538-3873/aae8ac)
- McCully, C., Volgenau, N. H., Harbeck, D.-R., et al. 2018, in Society of Photo-Optical Instrumentation Engineers (SPIE) Conference Series, Vol. 10707, Software and Cyberinfrastructure for Astronomy V, ed. J. C. Guzman & J. Ibsen, 107070K, doi: [10.1117/12.2314340](https://doi.org/10.1117/12.2314340)
- Meech, K. J., & Svoren, J. 2004, in Comets II, ed. M. C. Festou, H. U. Keller, & H. A. Weaver, 317
- Miles, R. 2016, Icarus, 272, 387, doi: [10.1016/j.icarus.2015.11.011](https://doi.org/10.1016/j.icarus.2015.11.011)
- Ootsubo, T., Kawakita, H., Hamada, S., et al. 2012, ApJ, 752, 15, doi: [10.1088/0004-637X/752/1/15](https://doi.org/10.1088/0004-637X/752/1/15)
- pandas development team, T. 2020, pandas-dev/pandas: Pandas, latest, Zenodo, doi: [10.5281/zenodo.3509134](https://doi.org/10.5281/zenodo.3509134)
- Peixinho, N., Thirouin, A., Tegler, S. C., et al. 2020, in The Trans-Neptunian Solar System, ed. D. Prialnik, M. A. Barucci, & L. Young, 307–329, doi: [10.1016/B978-0-12-816490-7.00014-X](https://doi.org/10.1016/B978-0-12-816490-7.00014-X)
- Prialnik, D. 1992, ApJ, 388, 196, doi: [10.1086/171143](https://doi.org/10.1086/171143)
- Reach, W. T., Kelley, M. S., & Vaubaillon, J. 2013, Icarus, 226, 777, doi: [10.1016/j.icarus.2013.06.011](https://doi.org/10.1016/j.icarus.2013.06.011)
- Rein, H., & Liu, S. F. 2012, A&A, 537, A128, doi: [10.1051/0004-6361/201118085](https://doi.org/10.1051/0004-6361/201118085)
- Rein, H., & Spiegel, D. S. 2015, MNRAS, 446, 1424, doi: [10.1093/mnras/stu2164](https://doi.org/10.1093/mnras/stu2164)
- Schleicher, D. 2010, Composite Dust Phase Function for Comets - Lowell Minor Planet Services
- Schleicher, D. G., Millis, R. L., & Birch, P. V. 1998, Icarus, 132, 397, doi: [10.1006/icar.1997.5902](https://doi.org/10.1006/icar.1997.5902)
- Schwamb, M. E., Jones, R. L., Yeomans, P., et al. 2023, ApJS, 266, 22, doi: [10.3847/1538-4365/acc173](https://doi.org/10.3847/1538-4365/acc173)
- Shubina, O., Kleshchonok, V., Ivanova, O., Luk'yanyk, I., & Baransky, A. 2023, Icarus, 391, 115340, doi: [10.1016/j.icarus.2022.115340](https://doi.org/10.1016/j.icarus.2022.115340)
- Smith, K. W., Smartt, S. J., Young, D. R., et al. 2020, PASP, 132, 085002, doi: [10.1088/1538-3873/ab936e](https://doi.org/10.1088/1538-3873/ab936e)
- Solontoi, M., Ivezić, Ž., Jurić, M., et al. 2012, Icarus, 218, 571, doi: [10.1016/j.icarus.2011.10.008](https://doi.org/10.1016/j.icarus.2011.10.008)
- Steele, I. A., Smith, R. J., Rees, P. C., et al. 2004, in Society of Photo-Optical Instrumentation Engineers (SPIE) Conference Series, Vol. 5489, Ground-based Telescopes, ed. J. Oschmann, Jacobus M., 679–692, doi: [10.1117/12.551456](https://doi.org/10.1117/12.551456)
- Tonry, J. L., Stubbs, C. W., Lykke, K. R., et al. 2012, ApJ, 750, 99, doi: [10.1088/0004-637X/750/2/99](https://doi.org/10.1088/0004-637X/750/2/99)
- Tonry, J. L., Denneau, L., Heinze, A. N., et al. 2018a, PASP, 130, 064505, doi: [10.1088/1538-3873/aabadf](https://doi.org/10.1088/1538-3873/aabadf)
- Tonry, J. L., Denneau, L., Flewelling, H., et al. 2018b, ApJ, 867, 105, doi: [10.3847/1538-4357/aae386](https://doi.org/10.3847/1538-4357/aae386)
- Trigo-Rodríguez, J. M., Davidsson, B., Montanes-Rodríguez, P., Sanchez, A., & Troughton, B. 2008, in 39th Annual Lunar and Planetary Science Conference, Lunar and Planetary Science Conference, 1627
- Trigo-Rodríguez, J. M., García-Hernández, D. A., Sánchez, A., et al. 2010, MNRAS, 409, 1682, doi: [10.1111/j.1365-2966.2010.17425.x](https://doi.org/10.1111/j.1365-2966.2010.17425.x)
- Trigo-Rodríguez, J. M., García-Melendo, E., Davidsson, B. J. R., et al. 2008, A&A, 485, 599, doi: [10.1051/0004-6361:20078666](https://doi.org/10.1051/0004-6361:20078666)
- Trigo-Rodríguez, J. M., Sánchez, A., Llenas, J. M., & Gritsevich, M. 2024, in LPI Contributions, Vol. 3040, 55th Lunar and Planetary Science Conference, 1363

- van der Walt, S., Colbert, S. C., & Varoquaux, G. 2011, Computing in Science and Engineering, 13, 22, doi: [10.1109/MCSE.2011.37](https://doi.org/10.1109/MCSE.2011.37)
- Van Rossum, G. 2020, The Python Library Reference, release 3.8.2 (Python Software Foundation)
- Virtanen, P., Gommers, R., Oliphant, T. E., et al. 2020, Nature Methods, 17, 261, doi: [10.1038/s41592-019-0686-2](https://doi.org/10.1038/s41592-019-0686-2)
- Willmer, C. N. A. 2018, ApJS, 236, 47, doi: [10.3847/1538-4365/aabfdf](https://doi.org/10.3847/1538-4365/aabfdf)
- Womack, M., Sarid, G., & Wierzbos, K. 2017, PASP, 129, 031001, doi: [10.1088/1538-3873/129/973/031001](https://doi.org/10.1088/1538-3873/129/973/031001)